DOI:
10.1088/1361-6560/aaf246

Document Version
Peer reviewed version

Joint cardiac and respiratory motion estimation for motion-corrected cardiac PET-MR

Christoph Kolbitsch[1,2], Radhouene Neji[2,3], Matthias Fenchel[4], Andreas Schuh[5], Andrew Mallia[2], Paul Marsden[2], and Tobias Schaeffter[1,2]

[1]Physikalisch-Technische Bundesanstalt (PTB), Braunschweig and Berlin, Germany

[2]King's College London, School of Biomedical Engineering and Imaging Sciences, London, UK

[3]MR Research Collaborations, Siemens Healthcare, Frimley, UK

[4]MR R&D Collaborations, Siemens Medical Solutions, New York, USA

[5]Biomedical Image Analysis Group, Department of Computing, Imperial College London, London, UK

Corresponding author:

Christoph Kolbitsch, Physikalisch-Technische Bundesanstalt (PTB), Abbestraße 2-12, 10587 Berlin, Germany, E-mail: christoph.kolbitsch@ptb.de

Short running title:

Joint PET-MR motion estimation

Word count: 5100

ABSTRACT

Respiratory and cardiac motion can strongly impair cardiac PET image quality and tracer uptake quantification. Standard gating techniques can minimize these motion artefacts but suffer from low signal-to-noise ratio because only a small percentage of the total data is utilized. Motion correction approaches have been proposed to overcome this problem but require accurate knowledge of such physiological motion. Here we present a joint PET-MR motion estimation approach which combines complimentary dynamic image information from simultaneously acquired MR and PET to ensure improved cardiac and respiratory motion estimation for motion-corrected image reconstruction (MCIR) of PET images.

A 3D triple-echo Dixon MR scan is used both for calculation of MR-based attenuation correction (AC) maps and estimation of physiological motion. PET listmode data is obtained simultaneously to the MR acquisition which is used for a joint motion estimation and reconstruction of the final MCIR PET. In a first step, dynamic cardiac and respiratory motion resolved 4D MR and PET images are reconstructed. These image series are used in a joint image registration to estimate non-rigid cardiac and respiratory motion fields. In a second step, the motion fields are utilized in a MR MCIR to obtain cardiac and respiratory resolved dynamic MR-based AC maps. In the last step, the non-rigid motion fields and the dynamic AC maps are applied in a PET MCIR to obtain the final motion-corrected PET images. PET-MR data has been obtained in six patients without any known heart disease. Motion amplitudes were between 5.6 and 16 mm, with higher values in the basal compared to the mid-ventricular and apical segments. The proposed joint PET-MR motion estimation provided more accurate motion estimation than using either modality separately. The underestimation of PET uptake due to respiratory and cardiac motion artefacts in the AC maps was up to 17%. The average increase in uptake values using MCIR was $23 \pm 10\%$ ($p<0.0001$), with values of $28 \pm 11\%$ ($p<0.0001$) for basal, $21 \pm 8\%$ ($p<0.0001$) for mid-cavity and $17 \pm 7\%$ ($p<0.0001$) for apical segments.

With the proposed scheme we could ensure high PET image quality and improve local PET uptake

quantification by up to 30%. Attenuation correction and motion information was obtained from the same PET-MR raw data, which was obtained during free-breathing to minimize scan times and to increase patient comfort.

INTRODUCTION

Simultaneous Positron Emission Tomography (PET) – Magnetic Resonance (MR) allows for the simultaneous acquisition of MR and PET data (Judenhofer et al. 2008; Gaa et al. 2004; Antoch & Bockisch 2009). It combines 3D high-resolution anatomical information of MRI with metabolic information obtained with PET. MRI can also provide additional diagnostic information such as tissue perfusion or tissue microstructure making PET-MR a highly promising multi-parametric imaging technique.

Commonly, acquisition times for one station 3D-PET and 3D high-resolution MRI are in the range of several minutes. Since both MR and PET data streams are obtained simultaneously, they are also affected by the same physiological motion, such as breathing or the heartbeat (Scott et al. 2009; Munoz et al. 2016; Catana 2015). Usually gating techniques are applied to restrict data acquisition or reconstruction to a predefined respiratory and cardiac phase to minimize motion artefacts. However, these methods often suffer from low signal-to-noise-ratio (SNR) because only a small percentage of the acquired data is used for the final image reconstruction. Instead, motion correction approaches can utilize all the acquired data while minimizing motion artefacts (Qiao et al. 2006; Dey 2010; Polycarpou et al. 2012) but require the knowledge of the underlying physiological motion. For this a range of techniques has been proposed which utilize the high soft tissue contrast of MR to detect and estimate organ displacement due to motion (Würslin et al. 2013; Fayad et al. 2015; Furst et al. 2015; Grimm et al. 2015; Manber et al. 2016; Rank et al. 2017; Kolbitsch et al. 2018a; Munoz et al. 2018). The resulting motion fields can then be used to improve image quality and quantification accuracy of simultaneously acquired PET data.

Compared to MRI, PET images commonly have a lower spatial resolution and provide image contrast only in regions where there is tracer uptake. Nevertheless, studies have shown that respiratory and cardiac motion can successfully be estimated from cardiac PET images (Gigengack et al. 2012; Lamare et al. 2014). We hypothesize that the complementary image information of MR and PET can improve

the estimation of organ displacements due to physiological motion compared to using either modality separately. Simultaneously acquired PET and MR data in a joint framework has previously been used to improve PET and MR images of the brain via multi-modality image regularization (Knoll et al. 2017; Ehrhardt et al. 2015; Mehranian et al. 2017) and to improve the estimation of respiratory motion (Fieseler et al. 2014; Fayad et al. 2015).

Here we present a joint PET-MR motion estimation framework which yields not just respiratory but also 3D non-rigid cardiac motion fields for motion-corrected image reconstruction (MCIR) in cardiac PET applications. A triple echo Dixon MR scan was carried out with a 3D Golden Radial Phase Encoding (GRPE) scheme, which allows for reconstruction of cardiac and respiratory resolved 3D images as well as the reconstruction of fat-water separated static images that are used for MR-based attenuation correction (AC) estimation from the same data (Kolbitsch et al. 2018a). The method was evaluated in six patients to investigate if the joint motion estimation yields a better MCIR-PET image quality than using either PET or MR data separately. In addition, we investigated the effect of cardiac and respiratory motion on the MR-based attenuation correction (AC) maps used for the MCIR-PET.

METHODS

An overview of the proposed method is given in Figure 1. In a first motion estimation step, simultaneously acquired GRPE MR and PET data are split into different cardiac and respiratory motion phases, followed by reconstruction of 4D dynamic images. Non-rigid cardiac and respiratory motion fields are then estimated from the 4D MR and PET data. In a second step, these 4D motion fields are used to reconstruct 3D MCIR MR images from the same raw data as above and to obtain dynamic MR-based AC maps. In a final step the motion fields and the dynamic AC maps are utilized to obtain MCIR PET images.

Data acquisition

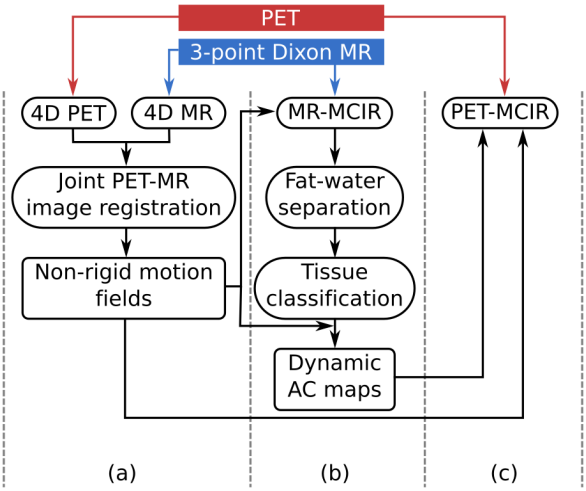

Figure 1: Overview of the proposed joint cardiac and respiratory motion correction approach. (a) Simultaneously acquired data was split into dynamic 4D motion resolved images. 4D non-rigid motion fields were estimated in a joint motion estimation framework. That step was repeated twice, once for respiratory and once for cardiac motion estimation. (b) Motion fields were utilized in a motion-corrected image reconstruction (MCIR) of the 3-point Dixon MR data with subsequent fat-water separation. Tissue types were classified and dynamic AC maps were calculated. (c) The non-rigid motion fields and the dynamic AC maps were then used in a MCIR to obtain the final motion corrected PET images.

GRPE is a highly flexible 3D sampling scheme which provides 3D high-resolution static images and allows for the reconstruction of motion-resolved 3D images (Prieto et al. 2010; Cruz et al. 2016). In combination with a regularized image reconstruction, GRPE ensures high image quality even for images reconstructed from very few RPE lines. GRPE has previously been used in a range of applications to estimate cardiac and respiratory motion for MR and PET-MR applications (Buerger et al. 2013; Kolbitsch et al. 2017).

For GRPE, data is obtained along parallel readout lines and phase encoding is carried out on a radial pattern. Supplemental figure 1 visualizes the GRPE sampling. All phase encoding points along one RPE line are acquired before the angle is increased. The angular increment between two successive lines is the Golden angle of 111.24°. This ensures a homogeneous coverage of k-space for an arbitrary number of RPE lines.

GRPE leads to a cylindrical field-of-view (FOV), where the height of the cylinder along foot-head-direction is covered by the readout direction and the phase encoding is carried out in the circular basis of the FOV (along anterior-posterior and left-right, respectively). This is in contrast to a radial stack-

of-stars trajectory, which also yields a cylindrical FOV but where the height of the cylinder corresponds to the slice-encoding direction rather than the readout (Grimm et al. 2015).

Motion-resolved reconstruction

Motion surrogates and data binning

The binning of MR and PET raw data into different cardiac phases was carried out using an external ECG device. The ECG signal was recorded during data acquisition and based on the detected R-peaks, data was split into eight different cardiac motion states.

The respiratory bins were defined based on a MR self-navigator signal which was calculated from the GRPE data using the same approach as presented in (Kolbitsch et al. 2018b). For each phase encoding point in the center of a RPE line ($k_y = k_z = 0$), a complete readout line is obtained. The image orientation in this study was sagittal. Therefore, the readout covers the foot-head direction of the subject and each central RPE line yields a 1D projection of the subject along the foot-head direction. Although the image information in this 1D projection is very limited, the respiratory movement of large organs such as the heart and the liver can be detected. A Principle Component Analysis (PCA)-based scheme is used to extract a quantitative self-navigator signal. Based on this surrogate signal, MR and PET data were binned into eight different respiratory motion states. Please refer to (Kolbitsch et al. 2018b) for a more detailed description of the calculation of the self-navigator.

Cardiac and respiratory binning was carried out independently to ensure sufficient data was available for each motion state.

Image reconstruction

The 4D dynamic respiratory and cardiac resolved MR GRPE data was reconstructed offline using an iterative non-Cartesian reconstruction approach implemented in MATLAB (The MathWorks, Inc., Natich, MA, USA). The changes of the anatomy over time in these 4D images is smooth and restricted to only parts of the FOV. In order to exploit the temporal similarity of successive time frames, total

variation regularization along the temporal direction was used during image reconstruction. In addition, spatial total variation regularization was added to further reduce undersampling artefacts and to ensure high image quality for motion estimation (Cruz et al. 2016).

The reconstruction of the dynamic PET data was carried out using STIR (Thielemans et al. 2012). A 3D ordered subsets expectation maximization (OSEM) algorithm was used with 23 subsets and three full iterations. The reconstructed matrix size was 127 x 344 x 344 pixel with an image resolution of 2 x 2.1 x 2.1 mm^3. Scatter correction is carried out iteratively based on single scatter estimation and upscaling using a tail-fit method. Scatter and random corrections are applied to each motion state separately. Normalisation of the PET raw data was carried out based on the standard normalisation file obtained from the PET-MR scanner. The reconstructed images were smoothed with a 6 x 6 x 6 mm^3 Gaussian kernel. Random and scatter correction was included in the image reconstruction. Image reconstruction was carried out first without the use of any attenuation correction in order to ensure that any mismatch between AC maps and dynamic PET data does not lead to artefacts which could impair the subsequent motion estimation.

Joint motion estimation

In order to obtain 3D non-rigid respiratory and cardiac motion transformations (T_i) which describe both the dynamic changes in the 4D MR and PET images, the following registration functional was defined:

$$\min_{T} \left((1-\lambda) S\left(I_i^{MR} \circ T_i, I_{ref}^{MR}\right) + \lambda S\left(I_i^{PET} \circ T_i, I_{ref}^{PET}\right) + \sigma B(T_i) \right) \qquad [1]$$

where S is the image difference metric (normalised mutual information) and I_i are the 3D images at different motion states i. For a given motion state i, the image difference between the current image I_i transformed with the estimated transformation T_i and the reference image I_{ref} is minimized. The reference motion states were defined as end-expiration and mid-diastole for respiratory and cardiac motion estimation, respectively. The above minimization was solved using a spline-based registration

approach (MIRTK, https://biomedia.doc.ic.ac.uk/software/mirtk/), where the regularization term *B* multiplied with the weighting factor σ ensures smooth transformation and robustness of the motion estimation in the presence of noise (Rueckert et al. 1999). The weighting between MR and PET image information is determined by λ, i.e. for $\lambda = 0$ only the MR image information is considered during the minimization and for $\lambda = 1$ only the PET image data. For the joint PET-MR motion estimation λ was set to 0.5 to give equal weight to MR and PET image information.

Image registration was carried out separately for the respiratory and cardiac resolved 4D MR and PET data yielding eight respiratory and eight cardiac transformations. Combining both respiratory and cardiac motion information provided eight respiratory and eight cardiac, i.e. overall 64 different transformations. The joint PET-MR image registration for eight respiratory or cardiac phases took ~10 minutes on a high-power computer with 24 CPU cores.

MR Motion-corrected reconstruction

For the final motion-corrected MR image reconstruction the MR raw data was separated into 64 (eight respiratory times eight cardiac) different motion states. The 64 motion transformations from above were then used during MCIR to obtain a single motion-corrected 3D image at end-expiration and mid-diastole for each echo time with improved image quality and signal-to-noise. The MR-MCIR algorithm was the same as used for the reconstruction of the 4D images, but the motion transformations are taken into consideration at each iteration step to minimize motion artefacts (Batchelor et al. 2005).

Attenuation correction maps

The MCIR MR images at three different echo times were then used to estimate the fat and water content for each pixel based on a quadratic pseudoboolean optimization (Berglund & Kullberg 2012). Using this separation, each tissue was classified as either soft tissue, fat, air or lung tissue. Literature-based values for attenuation coefficients were then assigned to the different tissue types: soft tissue

0.1 cm^{-1}, fat tissue 0.09 cm^{-1}, lung tissue 0.02 cm^{-1} and air 0 cm^{-1} in order to calculate the AC map (Martinez-Moller et al. 2009). For MCIR PET, the AC map were transformed using the estimated cardiac and respiratory motion transformations resulting in 64 AC maps at different motion states for each patient. That ensured, that the AC map is accurately aligned with the PET data of the different motion states during MCIR.

PET Motion-corrected reconstruction

Similar to MCIR MR approach, the 64 motion transformations were also included into a MCIR PET reconstruction to obtain a high quality 3D PET image at end-expiration and mid-diastole (Qiao et al. 2006; Dey 2010). MCIR PET was carried out with STIR with the same reconstruction parameters as for the 4D PET reconstruction but with a smaller Gaussian smoothing kernel (4-mm isotropic) and using the dynamic cardiac and respiratory motion resolved MR-based AC maps to obtain quantitative PET images.

Experiments

Simultaneous PET and triple echo Dixon MR data acquisitions were carried out over 3:18 min during free-breathing in six patients (4 males, 52 $\pm$ 10 y, 72 $\pm$ 13 kg). The patients had been referred to our hospital for a clinical PET-CT scan and were afterwards scanned additionally on a simultaneous PET-MR scanner (Biograph mMR, Siemens Healthcare, Erlangen, Germany) without any additional injection of tracer. For PET-CT imaging, patients were injected with 330 $\pm$ 29 MBq of ^{18}F-FDG and PET-MR imaging was carried out 162 $\pm$ 19 min after contrast injection.

For the MR scan a prototype triple echo Dixon GRPE sequence was used with a sagittal imaging orientation with the following parameters: FOV = 400 x 500 x 500 mm^3, TE = 1.2/2.7/4.2ms, FA = 10°, spatial resolution: 1.9 x 3.2 x 3.2 mm^3. For each GRPE line, 125 phase encoding points were acquired

leading to an acquisition time of ~750ms for one GRPE angle. In total, 256 GRPE lines at different angles were obtained. PET data was acquired in listmode simultaneous to the MR scan.

Evaluation

Accuracy of AC

Physiological motion leads to blurring of uptake structures in the PET images. In addition, motion also affects the MR images used for the calculation of the AC maps used for PET image reconstruction. Any artefacts in these MR images therefore can impair PET image quality and uptake quantification. In order to study this indirect effect of cardiac and respiratory motion, AC maps were obtained from GRPE MR images (a) without motion correction (AC_U), (b) only with respiratory motion correction (AC_R) and (c) with respiratory and cardiac motion correction ($AC_{R\&C}$). MCIR-PET images using AC_U, AC_R and $AC_{R\&C}$ were reconstructed and analyzed. The comparison of AC maps with and without respiratory motion correction has previously been presented in (Kolbitsch et al. 2018b) but without the proposed extension including cardiac motion correction.

Motion-corrected PET images

In order to evaluate the potential benefit of the proposed joint motion estimation, image registration according to Eq. 1 was carried out with $\lambda = 0$ and $\lambda = 1$, i.e. using only the MR and the PET image information, respectively. The obtained motion fields were then utilised in PET MCIR. For comparison purposes PET images were also reconstructed without motion correction with the same reconstruction parameters.

Quantitative Evaluation

To assess the effect of physiological motion on both PET emission data and AC maps, PET images were reformatted to short-axis orientation and then a quantitative bulls-eye analysis of the mean uptake in

each segment was calculated according to the standard of the American Heart Association (AHA) (Cerqueira 2002). In addition, the motion fields obtained with the proposed joint motion-estimation scheme were also reformatted in the same way and motion amplitudes were determined as an average over all basal, mid-ventricular and apical segments. Motion amplitudes were calculated as the length of the motion vectors between the reference motion phase (end-expiration mid-diastole) and the motion phase with the largest deformation (e.g. end-inspiration systole).

RESULTS

Motion-resolved reconstruction

Figure 2 shows the respiratory and cardiac resolved MR and PET images for one patient. Breathing mainly leads to a translation of the heart along the foot-head direction which is visible in both MR and PET images. The contraction of the myocardium is better visualized in the PET images. There was little image contrast between myocardium and blood in the 3D spoiled-gradient echo MR images and therefore the cardiac motion resolved MR images show the changes in the outline of the heart due to the heartbeat but not the thickening of the heart muscle.

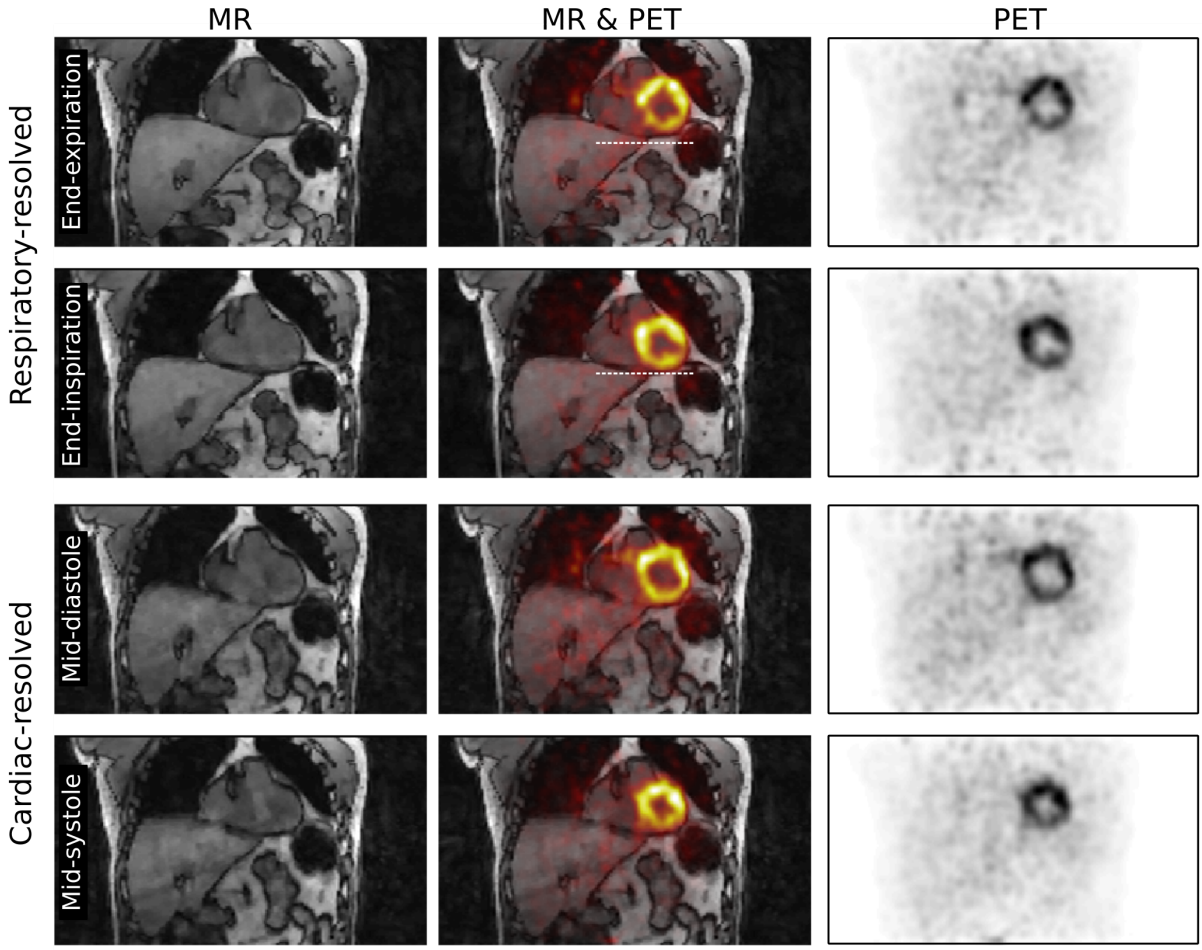

Figure 2: 4D MR and PET images showing respiratory and cardiac motion. Changes of the anatomy due to physiological motion can be clearly seen both in the MR and PET images.

Accuracy of AC maps

MR images reconstructed without motion correction, with respiratory and with joint respiratory and cardiac motion correction are shown in Figure 3 for two patients. Motion blurring due to breathing can be clearly seen at the dome of the liver (white arrows) which was compensated for by using respiratory MCIR. The outline of the heart was also improved with respiratory MCIR but residual blurring due to cardiac motion remains (blue arrows). Respiratory and cardiac MCIR further improved the visualization of the heart and led to a sharper delineation between the heart and its surrounding organs as can be observed along the line profiles.

Motion blurring in the MR images led to inaccurate calculation of MR-based AC maps. That was especially a problem at the border between heart and lung, because the AC values of lung are an order of magnitude smaller than the values for soft-tissue used for the heart.

The underestimation of the AC values in this lateral region of the heart led to an underestimation of PET uptake values when these AC maps were used in a MCIR PET reconstruction (Figure 4). The underestimation due to both respiratory and cardiac motion artefacts in the AC maps was up to 17%. For cardiac motion only, the underestimation was below 10% but still statistically significant over all patients for lateral segments.

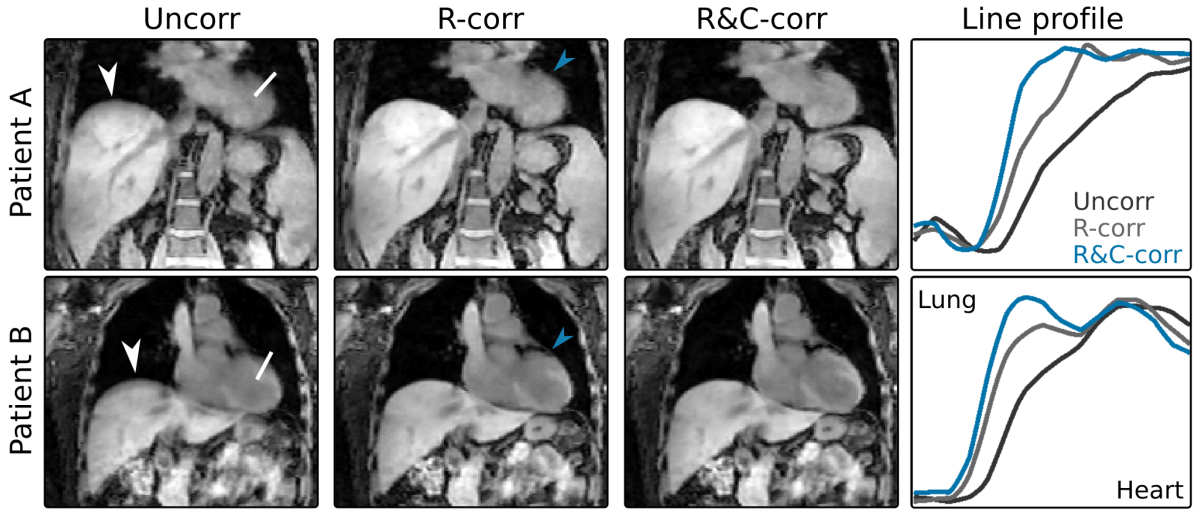

Figure 3: 3D GRPE MR images reconstructed without motion correction (Uncorr), with respiratory motion correction (R-corr) and with respiratory and cardiac motion correction (R&C-corr) for two patients. Line profiles taken from the top of the heart (location marked with white line in Uncorr) for all three images are also shown.

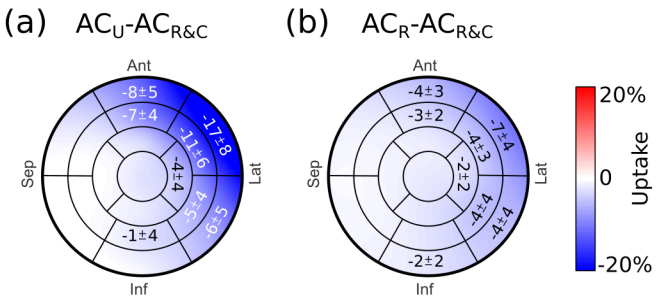

Figure 4: Bulls-eye plot of the difference in PET update calculated between the MCIR PET images (a) using AC_U and $AC_{R\&C}$ and (b) using AC_R and $AC_{R\&C}$. The underestimation of the outline of heart due to physiological motion shown in Figure 3 leads to an underestimation of PET uptake values. The bulls-eye plots only show segments with statistically significant differences over all patients.

Motion vector fields

Figure 5 compares motion vector fields for respiratory and cardiac motion estimation using only PET, only MR and the proposed joint PET-MR approach. PET-only motion estimation led to accurate motion information inside the heart but not for the surrounding tissue due to the lack of tracer uptake. MR-only motion estimation achieved good respiratory motion fields but does not capture cardiac motion due to the poor image contrast between blood and myocardium. The proposed approach ensured accurate cardiac and respiratory motion estimation of the heart and the surrounding tissue. This is also confirmed in Figure 6 which shows the motion amplitudes for each AHA segment for one patient over all eight respiratory and cardiac motion phases relative to the reference motion states. MR-only motion estimation underestimates cardiac motion leading to small motion amplitudes. PET-only motion estimation can be strongly affected by noise leading to large standard deviations of motion amplitudes and non-physiological motion estimates (e.g. motion amplitude of phase 3 larger than phase 4 and 5) (black arrows in Figure 6). Figure 7 shows the difference of the motion vector fields for different weighting factors λ compared to the motion vector fields obtained with $\lambda = 0.5$.

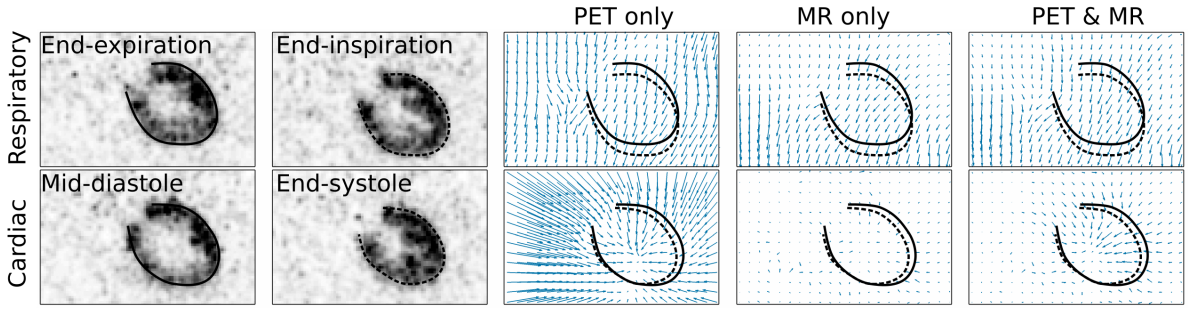

Figure 5: PET images and motion vector fields for respiratory and cardiac motion. Motion vector fields show the transformation from end-expiration to end-inspiration and mid-diastole to end-systole, respectively. Motion vector fields determined using only PET images (PET only), only MR images (MR only) and the proposed joint PET-MR motion estimation (PET & MR) are compared.

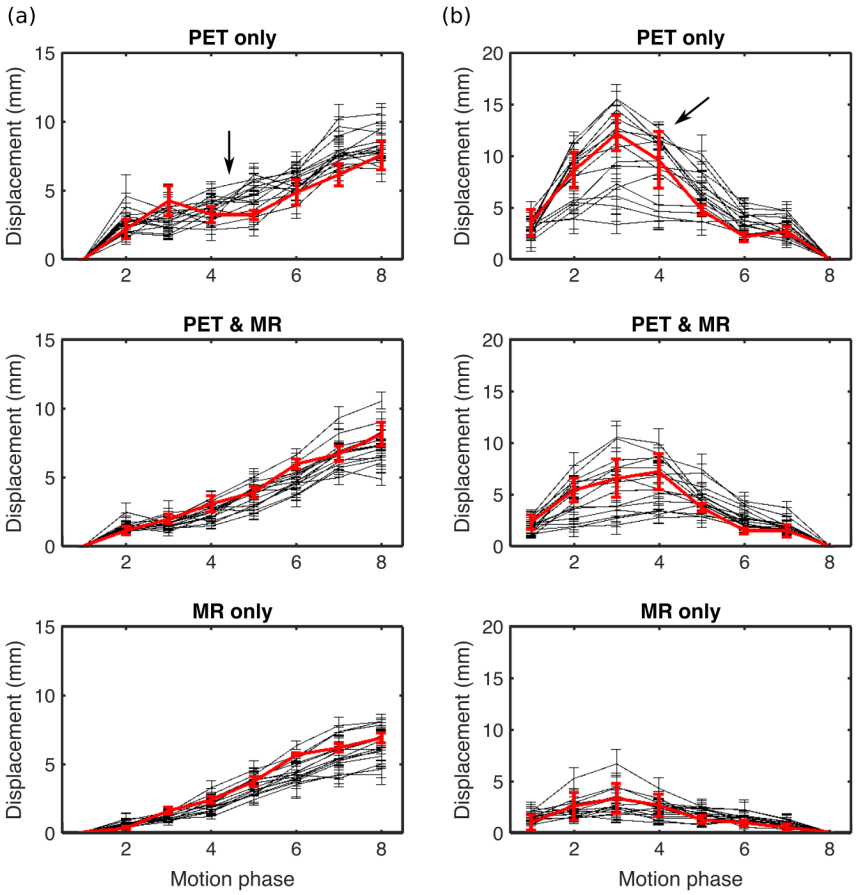

Figure 6: Respiratory (a) and cardiac (b) motion displacement relative to a reference phase (end-expiration (phase 1) and mid-diastole (phase 8), respectively) for one patient. Each line shows the average and standard deviation in one AHA segment over all eight motion phases.

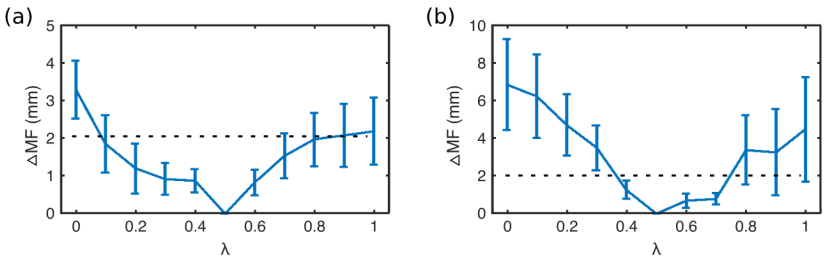

Figure 7: Difference of motion fields (ΔMF) for different weighting factors $\boldsymbol{\lambda}$ compared to $\boldsymbol{\lambda = 0.5}$ for respiratory (a) and cardiac (b) motion obtained in end-inspiration and systole, respectively. For $\boldsymbol{\lambda = 0}$ only MR image data and for $\boldsymbol{\lambda = 0}$ only PET image data is used for the motion estimation. The mean and standard deviation of the motion field difference were measured in a ROI in the heart of one patient. The dashed line indicates the spatial resolution of the PET images.

PET Motion-corrected reconstruction

MCIR PET images using motion fields obtained only from 4D PET images, only from 4D MR images and from the proposed joint PET-MR motion estimation are shown in Figure 8. Using only PET-based motion correction improved the quality of MCIR PET images but suffered from residual artefacts for example around the papillary muscles (black arrows in Figure 8). MR-based motion information could not fully correct for cardiac motion-induced blurring. The proposed PET-MR image registration could capture both types of motion and provided the best image quality.

An overview of all patients is given in Figure 9 showing cardiac and respiratory motion corrected MR and PET images. Uncorrected PET images are also shown for reference in order to demonstrate the higher PET image quality achieved with the proposed approach.

Figure 10 shows short-axis slices of four patients without and with motion correction using the respiratory and cardiac motion information obtained from PET and MR images. The visualization of the uptake in the myocardium and small structures such as the papillary muscles was strongly improved in all patients, which can also be seen in the line profiles drawn along the anterior-inferior direction of the heart.

A quantitative evaluation of the motion-corrected PET images is shown in Figure 11. Cardiac and respiratory motion correction led to an increase in measured uptake values in all segments, with a

higher increase in the basal segments compared to the apical segments. The average increase in uptake values over all patients was 23 ± 10% ($p<0.0001$), with values of 28 ± 11% ($p<0.0001$) for basal, 21 ± 8% ($p<0.0001$) for mid-cavity and 17 ± 7% ($p<0.0001$) for apical segments. Average motion amplitudes varied between 5.6 to 16 mm, with higher motion amplitudes in the basal compared to mid-ventricular and apical segments (Table 1).

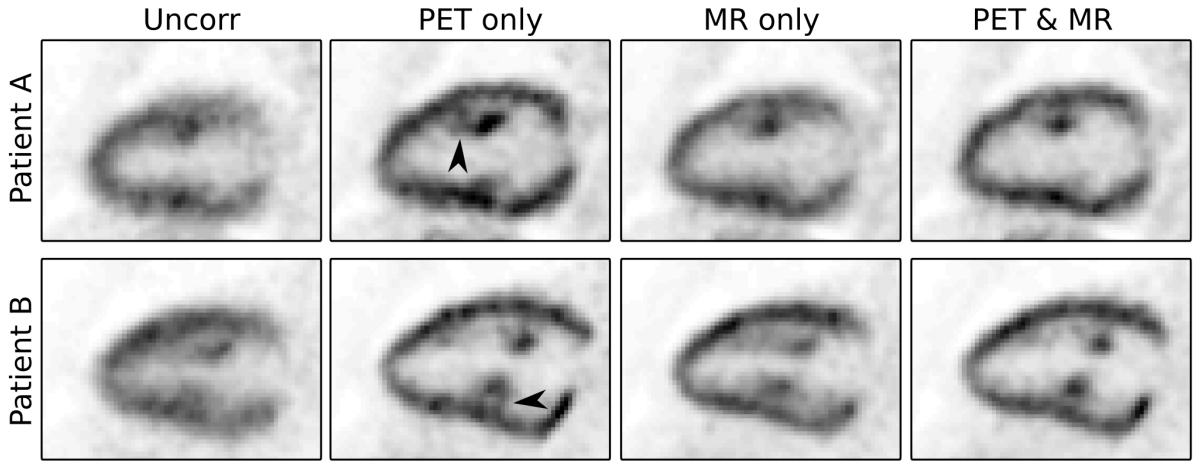

Figure 8: Long-axis slices of two patients comparing PET images without motion correction (Uncorr) and with cardiac and respiratory motion correction using motion fields obtained using only PET images (PET only), using only MR images (MR only) and the proposed joint PET-MR motion estimation (PET & MR). Artefacts (black arrows) and residual motion blurring is visible for motion correction based on PET only and MR only images.

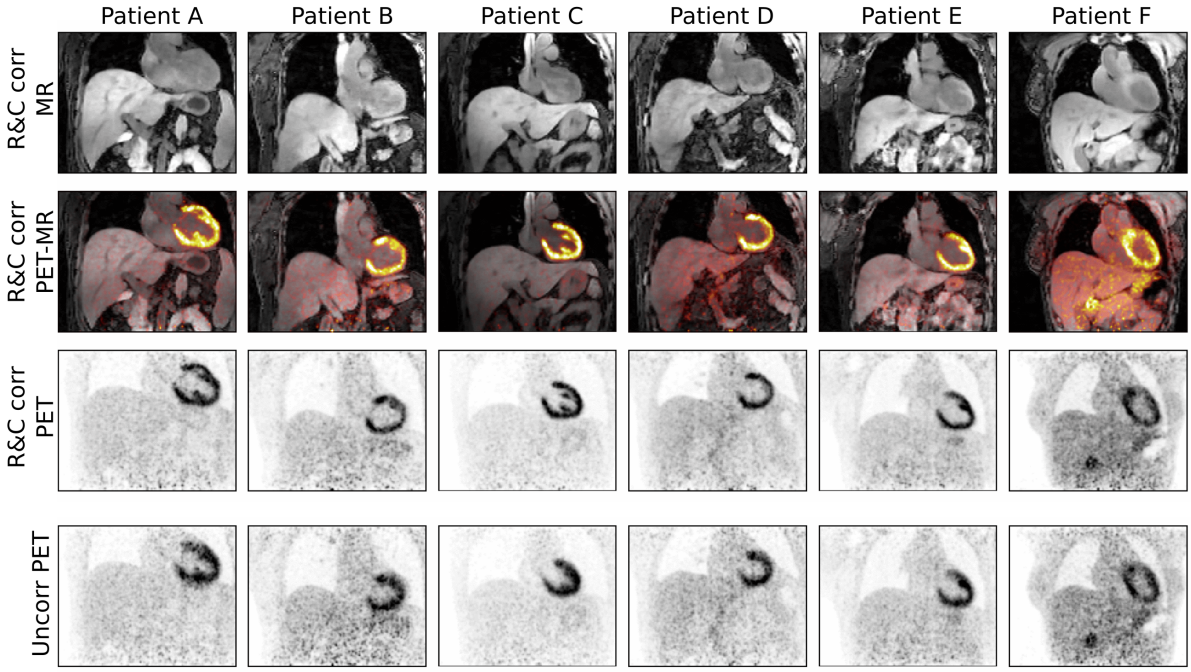

Figure 9: Results of all patients showing cardiac and respiratory motion corrected (R&C corr) MR and PET data. Ungated PET images without motion correction (uncorr) are also shown for comparison.

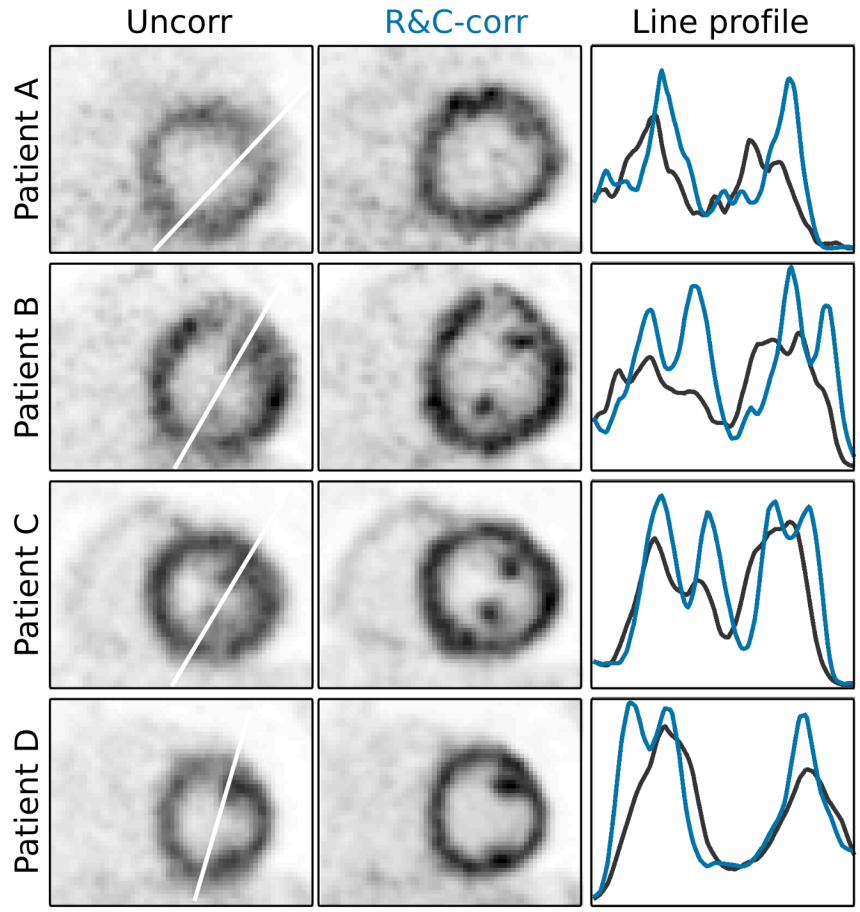

Figure 10: Short axis slices of four patients and line profiles drawn along the inferior-anterior direction of the heart comparing PET images without (Uncorr, black) and with respiratory and cardiac motion correction (R&C-corr, blue).

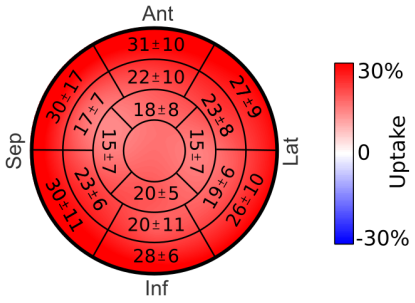

Figure 11: Bulls-eye plot of the relative difference in PET uptake values between the PET images without and with the proposed cardiac and respiratory motion correction.

Table 1: Summary of motion amplitudes and average change of PET uptake between the PET images without and with the proposed cardiac and respiratory motion correction approach. The changes in PET uptake is given relative to the PET images without motion correction. All values are given as averages ± standard deviation over all basal (B), mid-ventricular (M) and apical (A) segments.

Patient		1	2	3	4	5	6
Motion amplitude (mm)	A	12.1 ± 1.5	10.8 ± 2.8	10.7 ± 1.3	8.8 ± 1.8	8.4 ± 0.6	5.6 ± 1.0
	M	14.7 ± 1.3	11.1 ± 4.1	10.8 ± 2.6	11.0 ± 2.8	10.4 ± 1.3	5.7 ± 1.5
	B	16.0 ± 2.5	14.5 ± 4.2	12.3 ± 2.2	12.2 ± 2.7	12.0 ± 1.2	8.0 ± 2.2
Change of PET uptake (%)	A	20.0 ± 5.3	22.6 ± 3.5	8.1 ± 3.3	21.3 ± 5.9	17.1 ± 5.5	12.9 ± 3.2
	M	16.1 ± 5.7	27.6 ± 7.3	14.7 ± 7.3	23.2 ± 5.8	23.9 ± 10.1	19.2 ± 3.5
	B	27.1 ± 4.5	32.9 ± 6.4	24.0 ± 5.8	21.1 ± 7.9	37.2 ± 19.8	28.2 ± 4.5

DISCUSSION

With the proposed joint PET-MR motion estimation approach we were able to accurately estimate cardiac and respiratory motion, leading to improved PET image quality and quantification in all patients. The MR scan used in this study provided both physiological motion information and respiratory and cardiac motion-corrected AC maps.

Respiratory and cardiac motion led to shifts in the position of the heart and blurring of edges of the myocardium in the MR images. That caused bias in the estimation of the AC maps and an underestimation of PET uptake values even for the cardiac and respiratory motion-corrected PET images. The effect on measured PET uptake values depends strongly on the variation of the AC values in the affected region. Therefore, underestimation of uptake is most severe in the lateral region where the heart (attenuation coefficient of 0.1 cm^{-1}) is surrounded by lung tissue (attenuation coefficient of 0.02 cm^{-1}). With the proposed approach, cardiac and respiratory motion fields could also be utilized to minimize any motion artefacts in the MCIR AC maps and thus improve PET quantification accuracy.

The quantitative analysis shown in Figure 11 shows that the increase in measured uptake values between PET images without and with cardiac and respiratory motion correction depended on the slice position, with higher values for the basal segments compared to the apical segments. Estimated motion amplitudes varied in the same way. This is in good agreement with previous studies on cardiac motion (Scott et al. 2009). Although respiratory motion amplitudes have been reported to decrease from the apex to the middle of the right atrium by more than 25%, cardiac motion varies much more strongly. Motion amplitudes during the cardiac cycle are 70% smaller at the apex compared to the base of the heart. Higher motion amplitudes can result in stronger blurring of the PET uptake values in the uncorrected images and therefore a higher increase when using cardiac and respiratory motion correction.

Each of the motion-resolved PET images used to estimate respiratory and cardiac motion was reconstructed using part of the total acquired PET data and hence was very noisy. We selected the size of the Gaussian kernel to suppress this noise and make image registration more robust. Nevertheless, other approaches could be to use a stronger bending energy penalty in the registration functional.

For the in-vivo data no ground truth information is available, making a quantitative assessment of the obtained motion fields difficult. Nevertheless, the behavior of the motion amplitudes in Figure 6 suggest that PET-only is affected by the noise in the PET images leading to non-physiological motion estimates, e.g. non-linear behavior of motion amplitudes as a function of respiratory phase. This could also explain the residual motion artefacts in Figure 8.

Here we have used a weighting factor λ of 0.5, in order to give equal weight to the MR and PET image information. Figure 7 shows that the motion estimation varies slowly and smoothly with the weighting factor λ and any differences are below the spatial resolution of PET images for a wide range of λ. Nevertheless, further improvement could be achieved to use a spatially varying weighting factor $\lambda(x, y, z)$, e.g. based on PET uptake values. In order to accurately assess the optimal weighting factor,

an anatomically accurate PET-MR phantom which allows for the simulation of both respiratory and cardiac motion and yields realistic PET and MR image contrast needs to be developed.

The MR sequence used in this study was a 3D fast T1-weighted triple-echo Dixon sequence which provided both AC maps and physiological motion information. The T1 times of blood and myocardium are very similar and hence there was poor contrast between those two tissue types in MR images. That led to inaccurate MR-based cardiac motion estimation which was improved using the proposed joint PET-MR motion estimation. Other PET-MR studies have demonstrated accurate cardiac motion estimation using only MR images but they required the use of MR contrast agents to improve the contrast between blood and myocardium (Kolbitsch et al. 2017).

Our proposed approach utilizes the image information from simultaneously acquired MR and PET image data. Here MR and PET were obtained at the same time to ensure both modalities are affected by the same motion. For respiratory motion correction only, MR approaches have been proposed which require only 1 min scan time and can be used to correct PET data within a 45 min PET-MR protocol (Manber et al. 2015). PET image information only improves motion estimation, if there is tracer uptake in the moving structures. For tracers with very small uptake (e.g. ^{18}F-fluoride PET of the coronary arteries (Joshi et al. 2014)) an approach which relies only on MR motion estimation of the heart might be more accurate (Munoz et al. 2018).

Here we used a normalized mutual information metric for image registration of both MR and PET data. This metric has been used before for these modalities, but there is a range of other metrics such as sum-of-squared differences or residual complexity similarity measure which could be used instead (Lamare et al. 2014; Würslin et al. 2013; Gigengack et al. 2012; Buerger et al. 2011; Manber et al. 2015).

Using the objective function from Eq. 1 provides motion fields which describe both the changes in image content of MR and PET data. This is not the same as averaging an MR-only and PET-only motion

estimate, which can be seen in Figure 5. The large amplitudes in areas without PET uptake using PET-only do not impair the motion estimation of the joint PET-MR motion estimation.

CONCLUSION

We have demonstrated that utilizing both dynamic MR and PET image data to estimate cardiac and respiratory motion leads to a more robust motion estimation than using either data streams separately. With the proposed scheme we could ensure high PET image quality with accurate depiction also of small structures such as uptake in the papillary muscles and improved local PET uptake quantification by up to 30% without the need of cardiac gating. This ensured all the acquired PET data contributes to the final diagnostic image, maximizing the SNR of the PET images for a given scan duration. Dynamic 4D MR images and MR-based AC maps were obtained from the same raw data, minimizing the additional scan time required for motion estimation. This also allowed for the entire PET-MR scan to be carried out during free-breathing, increasing patient comfort.

ACKNOWLEDGEMENT

Dr. Neji and Dr. Fenchel are employees of Siemens Healthineers. This work was part of the SUBLIMA project supported by the European Union under the seventh framework program (no: 241711). This research was supported by the National Institute for Health Research (NIHR) Biomedical Research Centre at Guy's and St Thomas' NHS Foundation Trust and King's College London. The views expressed are those of the authors and not necessarily those of the NHS, the NIHR or the Department of Health. The PET image reconstruction used for this project was in part developed during the Computational Collaborative Project in Synergistic PET-MR Reconstruction (https://www.ccppetmr.ac.uk/), UK EPSRC grant EP/M022587/1. The authors would also like to thank James Stirling and Sami Jeljeli for their help with the patient scanning.

REFERENCES

Antoch, G. & Bockisch, A., 2009. Combined PET/MRI: a new dimension in whole-body oncology imaging? *European Journal of Nuclear Medicine*, 36 Suppl 1, pp.S113--20.

Batchelor, P.G. et al., 2005. Matrix description of general motion correction applied to multishot images. *Magnetic Resonance in Medicine*, 54(5), pp.1273–1280.

Berglund, J. & Kullberg, J., 2012. Three-dimensional water/fat separation and T2* estimation based on whole-image optimization-Application in breathhold liver imaging at 1.5 T. *Magnetic Resonance in Medicine*, 67, pp.1684–1693.

Buerger, C., Prieto, C. & Schaeffter, T., 2013. Highly efficient 3D motion-compensated abdomen MRI from undersampled Golden-RPE acquisitions. *Magma: Magnetic Resonance Materials in Physics, Biology, and Medicine*, 26(5), pp.419–429.

Buerger, C., Schaeffter, T. & King, A.P., 2011. Hierarchical adaptive local affine registration for fast and robust respiratory motion estimation. *Med Image Anal*.

Catana, C., 2015. Motion correction options in PET/MRI. *Seminars in Nuclear Medicine*, 45(3), pp.212–223.

Cerqueira, M.D., 2002. Standardized Myocardial Segmentation and Nomenclature for Tomographic Imaging of the Heart: A Statement for Healthcare Professionals From the Cardiac Imaging Committee of the Council on Clinical Cardiology of the American Heart Association. *Circulation*, 105(4), pp.539–542.

Cruz, G. et al., 2016. Accelerated motion corrected three-dimensional abdominal MRI using total variation regularized SENSE reconstruction. *Magnetic Resonance in Medicine*, 75(4), pp.1484–1498.

Dey, J., 2010. Reconstruction Algorithms for Motion Correction in Emission. *IEEE Trans Nucl*

Sci., 56(5), pp.2739–2749.

Ehrhardt, M.J. et al., 2015. Joint reconstruction of PET-MRI by exploiting structural similarity. *Inverse Problems*, 31(1), p.15001.

Fayad, H. et al., 2015. The use of a generalized reconstruction by inversion of coupled systems (GRICS) approach for generic respiratory motion correction in PET/MR imaging. *Physics in Medicine and Biology*, 60(6), pp.2529–2546.

Fieseler, M. et al., 2014. Motion correction of whole-body PET data with a joint PET-MRI registration functional. *Biomedical engineering online*, 13 Suppl 1(Suppl 1), p.S2.

Furst, S. et al., 2015. Motion Correction Strategies for Integrated PET/MR. *Journal of Nuclear Medicine*, 56(2), pp.261–269.

Gaa, J., Rummeny, E.J. & Seemann, M.D., 2004. Whole-body imaging with PET/MRI. *European Journal of Medical Research*, 9(6), pp.309–312.

Gigengack, F. et al., 2012. Motion Correction in Dual Gated Cardiac PET Using Mass-Preserving Image Registration. *IEEE Transactions on Medical Imaging*, 31(3), pp.698–712.

Grimm, R. et al., 2015. Self-gated MRI motion modeling for respiratory motion compensation in integrated PET/MRI. *Medical Image Analysis*, 19(1), pp.110–120.

Joshi, N. V. et al., 2014. 18F-fluoride positron emission tomography for identification of ruptured and high-risk coronary atherosclerotic plaques: A prospective clinical trial. *The Lancet*, 383(9918), pp.705–713.

Judenhofer, M.S. et al., 2008. Simultaneous PET-MRI: a new approach for functional and morphological imaging. *Nat. Med.*, 14(4), pp.459–465.

Knoll, F. et al., 2017. Joint MR-PET Reconstruction Using a Multi-Channel Image Regularizer.

IEEE Transactions on Medical Imaging, 36(1), pp.1–16.

Kolbitsch, C. et al., 2017. Cardiac and Respiratory Motion Correction for Simultaneous Cardiac PET/MR. *Journal of Nuclear Medicine*, 58(5), pp.846–852.

Kolbitsch, C. et al., 2018a. Fully integrated 3D high-resolution multicontrast abdominal PET-MR with high scan efficiency. *Magnetic Resonance in Medicine*, 79(2), pp.900–911.

Kolbitsch, C. et al., 2018b. Respiratory-resolved MR-based attenuation correction for motion-compensated cardiac PET-MR. *Physics in Medicine & Biology*, 63(13), p.135008.

Lamare, F. et al., 2014. Evaluation of respiratory and cardiac motion correction schemes in dual gated PET/CT cardiac imaging. *Medical physics*, 41(7), p.72504.

Manber, R. et al., 2016. Joint PET-MR respiratory motion models for clinical PET motion correction. *Physics in Medicine and Biology*, 61(17), pp.6515–6530.

Manber, R. et al., 2015. Practical PET Respiratory Motion Correction in Clinical PET/MR. *Journal of Nuclear Medicine*, 56(6), pp.890–896.

Martinez-Moller, A. et al., 2009. Tissue Classification as a Potential Approach for Attenuation Correction in Whole-Body PET/MRI: Evaluation with PET/CT Data. *Journal of Nuclear Medicine*, 50(4), pp.520–526.

Mehranian, A. et al., 2017. PET image reconstruction using multi-parametric anato-functional priors. *Physics in Medicine & Biology*, 62(15), pp.5975–6007.

Munoz, C. et al., 2018. Motion-corrected simultaneous cardiac positron emission tomography and coronary MR angiography with high acquisition efficiency. *Magnetic Resonance in Medicine*, 79(1), pp.339–350.

Munoz, C. et al., 2016. MR-Based Cardiac and Respiratory Motion-Compensation Techniques for PET-MR Imaging. *PET Clinics*, 11(2), pp.179–191.

Polycarpou, I., Tsoumpas, C. & Marsden, P.K., 2012. Analysis and comparison of two methods for motion correction in PET imaging. *Medical physics*, 39(10), pp.6474–6483.

Prieto, C. et al., 2010. 3D Undersampled Golden-Radial Phase Encoding for DCE-MRA Using Inherently Regularized Iterative SENSE. *Magnetic Resonance Imaging*, 64, pp.514–526.

Qiao, F. et al., 2006. A motion-incorporated reconstruction method for gated PET studies. *Phys Med Biol*, 51(15), pp.3769–3783.

Rank, C.M. et al., 2017. 4D respiratory motion-compensated image reconstruction of free-breathing radial MR data with very high undersampling. *Magnetic Resonance in Medicine*, 77(3), pp.1170–1183.

Rueckert, D. et al., 1999. Nonrigid registration using free-form deformations: application to breast MR images. *IEEE Transactions on Medical Imaging*, 18(8), pp.712–721.

Scott, A.D., Keegan, J. & Firmin, D.N., 2009. Motion in cardiovascular MR imaging. *Radiology*, 250(2), pp.331–351.

Thielemans, K. et al., 2012. STIR: software for tomographic image reconstruction release 2. *Phys Med Biol*, 57(4), pp.867–883.

Würslin, C. et al., 2013. Respiratory Motion Correction in Oncologic PET Using T1-Weighted MR Imaging on a Simultaneous Whole-Body PET/MR System. *Journal of Nuclear Medicine*, 54(3), pp.464–471.